

# Electron Acceleration and Time Variability of High Energy Emission from Blazars

Masaaki Kusunose

*Department of Physics, School of Science, Kwansai Gakuin University,  
Nishinomiya 662-8501, Japan*

kusunose@kwansai.ac.jp

Fumio Takahara

*Department of Earth and Space Science, Graduate School of Science, Osaka University,  
Toyonaka, Osaka 560-0043, Japan*

and

Hui Li

*Theoretical Astrophysics (T-6, MS B288), Los Alamos National Laboratory,  
Los Alamos, NM 87545*

## ABSTRACT

Blazars are known to emit a broad band emission from radio to gamma-rays with rapid time variations, particularly, in X- and gamma-rays. Synchrotron radiation and inverse Compton scattering are thought to play an important role in emission and the time variations are likely related to the acceleration of nonthermal electrons. As simultaneous multiwavelength observations with continuous time spans are recently available, some characteristics of electron acceleration are possibly inferred from the spectral changes of high energy emission. In order to make such inferences, we solve the time-dependent kinetic equations of electrons and photons simultaneously using a simple model for electron acceleration. We then show how the time variations of emission are dependent on electron acceleration. We also present a simple model for a flare in X-rays and TeV gamma-rays by temporarily changing the acceleration timescale. Our model will be used, in future, to analyze observed data in detail to obtain information on electron acceleration in blazars.

*Subject headings:* BL Lacertae objects: general – gamma rays: theory – radiation mechanisms: nonthermal

## 1. INTRODUCTION

High energy emission from blazars is usually thought to be produced by relativistically moving jets or blobs from the nucleus of galaxies (e.g., Blandford & Rees 1978; Blandford & Königl 1979; Maraschi, Ghisellini, & Celotti 1992; Sikora, Begelman, & Rees 1994; Inoue & Takahara 1996). The physical properties of such jets have been probed mostly based on the steady state models of synchrotron radiation and inverse Compton scattering by a nonthermal electron population (SSC model). However, blazars are also characterized by rapid and strong time variability. Recent observations have revealed that the emission exhibits short time variations in X- and gamma-ray bands on timescales from weeks down to half an hour (e.g., Mukherjee et al. 1997; Ulrich, et al. 1997, for review), as fast time variations of Mrk 421 were observed by X-rays and TeV gamma-rays (Gaidos et al. 1996; Takahashi et al. 1996); similar time variations of Mrk 501 were also found by multiwavelength observations (Kataoka et al. 1999). These observations should provide important clues on physical processes in relativistic jets, in particular, on electron acceleration.

To make theoretical inferences, we need to calculate time-dependent emission spectra from a time-dependent electron population. An example of such theoretical models was recently presented by Mastichiadis & Kirk (1997). They solved the kinetic equations of electrons and photons simultaneously, by injecting power-law electrons with an exponential cutoff. They showed various possibilities to explain the time variations observed from Mrk 421, such as the changes in the magnetic field or the maximum Lorentz factor of nonthermal electrons. Although the correlation between X-rays and TeV gamma-rays are important to discuss the SSC model, their estimate of Compton scattering in the Klein-Nishina regime does not necessarily correctly account for the energy change in scatterings, because of a simplified treatment of Compton scattering in the Klein-Nishina regime [see Mastichiadis & Kirk (1995) for the details of their calculation method]. Kirk et al. (1998), on the other hand, extended the above model, assuming that an acceleration region and a cooling region are spatially separated; i.e., electrons accelerated in a shock region are transferred to a cooling region where they emit synchrotron photons (they did not include Compton scattering). Their model was intended to explain the time variability of X-rays, by changing acceleration timescale.

Besides the time variations of flare activities explained by Mastichiadis & Kirk (1997) and Kirk et al. (1998), the early stages of acceleration are of great importance. By examining the properties of the time evolutions of photon spectra during acceleration, we may obtain the diagnoses of acceleration mechanisms. The recent development of observations in X-rays (ASCA and Beppo-SAX) to TeV gamma-rays (e.g., Whipple and HEGRA) and future experiments might be used to confirm the diagnoses.

In this paper, we use a formulation similar to Mastichiadis & Kirk (1997), but with the full Klein-Nishina cross section in the Compton scattering kernel, so that the emission in the TeV range is calculated correctly. We also include a particle acceleration process by considering spatially separated acceleration and cooling regions as in Kirk et al. (1998), although we do not consider

the spatial transfer of electrons. We particularly emphasize the detailed study of the properties of electron and photon spectra in the early stage of acceleration.

We describe our model in §2 and present numerical results in §3. Summary of our results is given in §4.

## 2. MODEL

### 2.1. Acceleration and Cooling Regions

We assume that observed photons are emitted from a blob moving relativistically towards us with Doppler factor  $\mathcal{D} = [\Gamma(1 - \beta_\Gamma\mu)]^{-1}$ , where  $\Gamma$  is the Lorentz factor of the blob,  $\beta_\Gamma$  is the speed of the blob in units of light speed  $c$ , and  $\mu$  is the cosine of the angle between the line of sight and the direction of motion of the blob. The blob is a spherical and uniform cloud with radius  $R$ , except that the blob includes an acceleration region which is presumably a shock front. It is assumed that the spatial volume of the acceleration region is small, and that the acceleration region is a slab with thickness  $R_{\text{acc}}$  defined below. The spectra of electrons and photons in the blob are calculated for the acceleration and cooling regions separately by solving equations described in §2.2.

We assume that the acceleration region (hereafter AR) and the cooling region (hereafter CR) are spatially separated; shocks in the blob are expected to be the site of electron acceleration and electrons cool mainly outside the shock regions. In the AR, electrons are mainly accelerated and cooling is unimportant except for the highest value of  $\gamma$ , while, in the CR, electrons with a nonthermal spectrum are injected from the AR; the escape rate of electrons from the AR is equal to the injection rate of electrons in the CR because of the number conservation. We further assume that acceleration time,  $t_{\text{acc}}$ , and escape time,  $t_{e,\text{esc}}$ , in the AR are energy independent as given in equation (4) below. With these assumptions, the number spectrum of electrons in the AR is a power law with a power-law index  $-2$ , i.e.,  $N(\gamma) \propto \gamma^{-2}$ , which is confirmed analytically (e.g., Kirk et al. 1998). Thus the maximum energy of electrons is determined by the balance of cooling and acceleration. Since we consider  $t_{\text{acc}} \ll R/c$  (see §3.1), the size of the AR is much smaller than the size of the blob itself.

We use this formulation because  $N(\gamma) \propto \gamma^{-2}$  is expected from the theory of shock acceleration (e.g., Druly 1983; Blandford & Eichler 1987). We, however, do not solve the spatial transfer of electrons as was done by Kirk et al. (1998). Instead, we simply calculate escaping electrons from the AR and put them into the CR. Although this may be an oversimplified model for realistic situations, the actual geometrical situation of shocks is not well known, either. Strictly speaking, our formulation is valid when ARs and CRs are more or less uniformly distributed in a cloud, but it is expected to be a fair approximation to the case where a single shock propagates in a jet as was studied by Kirk et al. (1998). As for the calculation of photon spectra, photons originating from one region penetrate into the other region but most of the photons originate from the CR

since the size of the AR is small. Thus, the electron cooling in the blob is governed either by its own magnetic field or by synchrotron photons stemming from the CR. We treat appropriately this situation in numerical calculations.

## 2.2. Kinetic Equations

The equation describing the time-evolution of the electron number spectrum in the AR is given by

$$\frac{\partial N(\gamma)}{\partial t} = -\frac{\partial}{\partial \gamma} \left\{ \left[ \left( \frac{d\gamma}{dt} \right)_{\text{acc}} - \left( \frac{d\gamma}{dt} \right)_{\text{loss}} \right] N(\gamma) \right\} - \frac{N(\gamma)}{t_{e,\text{esc}}} + Q(\gamma), \quad (1)$$

where  $\gamma$  is the Lorentz factor of electrons and  $N(\gamma)$  is the number density of electrons per unit  $\gamma$ . We assume that monochromatic electrons with Lorentz factor  $\gamma_0$  are injected in the AR, i.e.,  $Q(\gamma) = Q_0 \delta(\gamma - \gamma_0)$ . Electrons are then accelerated and lose energy by synchrotron radiation and Compton scattering; the energy loss rate is denoted by  $(d\gamma/dt)_{\text{loss}}$ . The acceleration term is approximated by

$$\left( \frac{d\gamma}{dt} \right)_{\text{acc}} = \frac{\gamma}{t_{\text{acc}}}. \quad (2)$$

In the framework of diffusive shock acceleration (e.g., Druly 1983; Blandford & Eichler 1987),  $t_{\text{acc}}$  can be approximated as

$$t_{\text{acc}} = \frac{20\lambda(\gamma)c}{3v_s^2} \sim 3.79 \times 10^{-6} \left( \frac{0.1\text{G}}{B} \right) \xi \gamma \text{ sec}, \quad (3)$$

where  $v_s \approx c$  is the shock speed,  $B$  is the magnetic field, and  $\lambda(\gamma) = \gamma m_e c^2 \xi / (eB)$  is the mean free path assumed to be proportional to the electron Larmor radius with  $\xi$  being a parameter,  $m_e$  the electron mass, and  $e$  the electron charge. Although this expression is valid only for test particle approximation in non-relativistic shocks, we rely on this since the basic dependences are not much changed in general cases.

For the convenience of numerical calculations, we assume  $t_{\text{acc}}$  does not depend on  $\gamma$ :

$$t_{\text{acc}} = 3.79 \times 10 \left( \frac{0.1\text{G}}{B} \right) \left( \frac{\gamma_f}{10^7} \right) \xi \text{ sec}, \quad (4)$$

where  $\gamma_f$  is assumed to be a characteristic Lorentz factor of relativistic electrons and used as a parameter; we set  $\gamma_f = 10^7$  throughout this paper. Although realistic acceleration time for the smaller values of  $\gamma$  should be correspondingly shorter, we make this choice because we mainly concern about the electrons with the large values of  $\gamma$ . One worry about this choice is the effect on the spectrum of accelerated electrons. We make sure that the resultant spectrum is that expected in diffusive shock acceleration by choosing  $t_{e,\text{esc}} = t_{\text{acc}}$  in the AR; this assumption of  $t_{e,\text{esc}} = t_{\text{acc}}$  is the same as used by Mastichiadis & Kirk (1995) in their proton acceleration model.

The electron spectrum in the CR is calculated by equation (1), with  $(d\gamma/dt)_{\text{acc}}$  dropped. Also  $Q(\gamma)$  is replaced by the escaping electrons from the AR and  $t_{e,\text{esc}}$  is set to be  $2R/c$ . The assumption

of  $2R/c$  in estimating  $t_{e,\text{esc}}$  is merely based on that electrons escaping from the blob take longer time than photons, and this point needs further work.

The relevant equation for the time evolution of photons is given by

$$\frac{\partial n_{\text{ph}}(\epsilon)}{\partial t} = \dot{n}_{\text{C}}(\epsilon) + \dot{n}_{\text{em}}(\epsilon) - \dot{n}_{\text{abs}}(\epsilon) - \frac{n_{\text{ph}}(\epsilon)}{t_{\gamma,\text{esc}}}, \quad (5)$$

where  $n_{\text{ph}}(\epsilon)$  is the photon number density per unit energy  $\epsilon$ . Compton scattering is calculated as

$$\dot{n}_{\text{C}}(\epsilon) = -n_{\text{ph}}(\epsilon) \int d\gamma N(\gamma) R_{\text{C}}(\epsilon, \gamma) + \int \int d\epsilon' d\gamma P(\epsilon; \epsilon', \gamma) R_{\text{C}}(\epsilon', \gamma) n_{\text{ph}}(\epsilon') N(\gamma), \quad (6)$$

using the exact Klein-Nishina cross section. First term of equation (6) denotes the rate that photons with energy  $\epsilon$  are scattered by electrons with the number spectrum  $N(\gamma)$ ;  $R_{\text{C}}$  is the angle-averaged scattering rate. Second term of equation (6) denotes the spectrum of scattered photons:  $P(\epsilon; \epsilon', \gamma)$  is the probability that a photon with energy  $\epsilon'$  is scattered by an electron with energy  $\gamma$  to have energy  $\epsilon$ . The probability  $P$  is normalized such that  $\int P(\epsilon; \epsilon', \gamma) d\epsilon = 1$ . The details of  $R_{\text{C}}$  and  $P$  are given in Jones (1968) and Blandford & Coppi (1990).

Photon production and self-absorption by synchrotron radiation are included in  $\dot{n}_{\text{em}}(\epsilon)$  and  $\dot{n}_{\text{abs}}(\epsilon)$ , respectively. The synchrotron emissivity and absorption coefficient are calculated based on the approximations given in Robinson & Melrose (1984) for mildly relativistic electrons and Crusius & Schlickeiser (1986) for relativistic electrons. External photon sources are not included. The rate of photon escape is estimated as  $n_{\text{ph}}(\epsilon)/t_{\gamma,\text{esc}}$ . We set  $t_{\gamma,\text{esc}} = R_{\text{acc}}/c$  and  $R/c$  in the AR and CR, respectively, because the scattering depth of the blob is much smaller than unity.

The comoving quantities are transformed back into the observer's frame depending on the Doppler factor and the redshift  $z$ ;  $\epsilon_{\text{obs}} = \epsilon \mathcal{D}/(1+z)$ , and  $dt_{\text{obs}} = dt(1+z)/\mathcal{D}$

### 3. RESULTS

We first examine the case where the cloud is initially empty and the injection of electrons starts at  $t = 0$ . The distribution function of the injected electrons is mono-energetic: Here  $\gamma_0 = 2$  is assumed. The strength of magnetic fields is assumed to have the same value both in ARs and in CRs, which is 0.1 G except in §3.4. Other parameters are redshift  $z = 0.05$ , Hubble constant  $H_0 = 75 \text{ km sec}^{-1} \text{ Mpc}^{-1}$ , and Doppler factor  $\mathcal{D} = 10$ . We also assume that the size of a cloud is measured by the timescale of variability, which is assumed to be  $R/(c\mathcal{D}) = 5 \times 10^4 \text{ sec}$  in the observer's frame.

#### 3.1. Time Evolution in Early Phase

First we simulate the time evolution from  $t = 0$  to  $R/c$  to study the evolution in an early stage. We assume  $\xi = 5 \times 10^2$  (i.e.,  $t_{\text{acc}} \approx 1.9 \times 10^4 \text{ sec}$  in the blob frame), and injection duration  $t = 0 -$

$R/c$ . In the CR, the escape time of electrons is assumed to be  $2R/c$ . The size of the AR is assumed to be  $R_{\text{acc}} = ct_{\text{acc}}/2$ . (Note that, in sections below, when we change the value of  $t_{\text{acc}}$ ,  $R_{\text{acc}}$  is also changed accordingly.) The injection rate of electrons in the AR is  $0.1 \text{ electrons cm}^{-3} \text{ sec}^{-1}$ . The volume of the AR is  $\sim 2.1 \times 10^{47} \text{ cm}^3$  and the total injection rate is  $\sim 2.1 \times 10^{46} \text{ electrons sec}^{-1}$ , assuming that the AR is approximated by a disk with radius  $R$  and thickness  $R_{\text{acc}}$ . The total power of electrons amounts to  $\sim 5 \times 10^{41} \text{ ergs sec}^{-1}$  by acceleration, if the power-law spectrum with an index of 2 is realized between  $\gamma_{\text{min}}$  and  $\gamma_{\text{max}}$ ; the minimum and maximum Lorentz factors  $\gamma_{\text{min}}$  and  $\gamma_{\text{max}}$  are tentatively taken to be 2 and  $3 \times 10^6$ , respectively.

In Figure 1, the evolution of the electron number spectrum is shown both for an AR and a CR. It is seen that electrons injected with the Lorentz factor 2 are gradually accelerated and the value of  $\gamma_{\text{max}}$  increases with time, where we take the value of  $\gamma_{\text{max}}$  such that  $N(\gamma) = 0$  for  $\gamma > \gamma_{\text{max}}$ . The value of  $\gamma_{\text{max}}$  in a steady state is determined by the balance among  $t_{\text{acc}}$ ,  $t_{e,\text{esc}}$ , and cooling time  $t_{\text{cool}}$  in the AR. Because we assume  $t_{\text{acc}} = t_{e,\text{esc}}$  in the AR,  $\gamma_{\text{max}}$  is simply determined by  $t_{\text{acc}}$  and  $t_{\text{cool}}$ . The value of  $\gamma_{\text{max}}$  in Figure 1 is  $\sim 4 \times 10^6$ . The spectrum reaches almost a steady state within  $R/c$ , which is a power law,  $N(\gamma) \propto \gamma^{-2}$ ; note that  $t_{\text{acc}} \sim 2 \times 10^4 \text{ sec}$  and  $R/c = 5 \times 10^5 \text{ sec}$  in the comoving frame of the blob for the present model.

In the CR, the effect of electron escape is negligible in the time interval shown in Figure 1, because the simulation is terminated at  $t = R/c$  while  $t_{e,\text{esc}} = 2R/c$ . Because of radiative cooling, a break  $\gamma_{\text{br}}$  appears at around  $3 \times 10^5$ . This break moves to lower energy when the evolution is continued until a steady state is attained;  $\gamma_{\text{br}} \sim 10^4$  at  $t = 10R/c$ . There is also a slight deceleration of electrons by cooling, which is shown by curves below  $\gamma = 2$ .

The spectral energy distribution (SED) of emission from the CR is shown in Figure 2; the flux and the photon energy are plotted in the observer's frame. Curves in the figure show the time evolution, with equally spaced time interval for  $t = 0 - R/c$  by solid curves. They evolve from lower to upper curves. In this stage, the synchrotron radiation dominates, because Compton scattering needs a timescale  $\sim R/c$  to be effective. SED at  $t = 2R/c$  (dotted curve) and  $10R/c$  (dashed curve) are also shown in the figure; here electrons are continuously injected until  $t = 10R/c$ . As shown by those curves, when the evolution is continued after  $R/c$ , the Compton component continues to increase before reaching a steady state. The peak energy of synchrotron emission initially increases but begins to decrease after about  $0.8R/c$  because electrons with  $\gamma < \gamma_{\text{br}}$  continue to accumulate and the value of  $\gamma_{\text{br}}$  decreases while those with  $\gamma > \gamma_{\text{br}}$  are saturated because of radiative cooling. After  $t = 2R/c$  the effects of electron escape begin to further modify the synchrotron spectrum; the intensity at the high energy part decreases while that at low energy still continues to increase slightly.

For  $t = 0 \sim R/c$ , light curves in the X-ray range are shown in Figure 3. Hard X-rays become dominant after  $t \sim 15t_{\text{acc}}$ , where  $t_{\text{acc}}/\mathcal{D} \sim 2 \times 10^3 \text{ sec}$  in the observer's frame.

The time evolution of the energy densities of electrons and photons in the CR are shown in Figure 4: The energy densities in the AR are comparable with those in the CR for the parameters

we used. In the CR,  $t_{e,\text{esc}} = 2R/c$  and  $t_{\gamma,\text{esc}} = R/c$  are assumed, so that the energy density of electrons is larger than that of photons. As was mentioned above, first the synchrotron photon energy-density rapidly increases and later the Compton photon energy-density (indicated by SSC in the figure) increases. It should be noted that the ratio of the energy densities of the Compton component to the synchrotron component is about 0.7 in the final stage, while the ratio of energy densities of synchrotron photons to magnetic fields is about 9. This is because the energy range of the target photons of Compton scattering is only a part of the synchrotron spectrum due to the Klein-Nishina limit. This result implies that we should be cautious about the estimate of the magnetic field strength from observations; if we simply estimate the magnetic field by multiplying the energy density of synchrotron photons by the ratio of synchrotron luminosity to Compton luminosity, it results in a large overestimation of magnetic field.

The energy injected through the electron acceleration is finally carried away by electrons and photons from the blob. The ratio of the amounts of the energies carried by electrons and photons is about 1.8 : 1 in a steady state (i.e.,  $t \sim 10R/c$ ). That is, electrons carry more jet power than radiation in this specific model.

The trajectories in the energy-flux *vs.* photon-index plane are shown for  $t = 0 - 10R/c$  in Figure 5 for various energy bands. Because the value of  $\gamma_{\text{max}}$  decreases due to radiative cooling, the flux of X-rays decreases when  $t >$  a few  $R/c$ . The flux of gamma-rays, on the other hand, continues to increase because of Compton scattering (see Figure 2).

### 3.2. Dependence on Acceleration Timescale

By changing the value of  $\xi$ , we compare the electron spectrum for different values of the acceleration time, where we keep  $t_{\text{acc}} = t_{e,\text{esc}}$  in the AR. In Figure 6, steady-state distributions of electrons for different values of  $\xi$  are compared. When the acceleration time scale is longer, the value of  $\gamma_{\text{max}}$  is reduced because of radiative cooling in the AR. Consequently, the emission spectrum becomes softer (Figure 7). It should be noted that because a smaller value of  $\xi$  leads to a smaller value of  $R_{\text{acc}}$  in our model, the luminosity from a blob becomes smaller when  $\xi$  is smaller. The extreme limit of  $\xi = 1$  corresponding to the Böhm limit results in the most efficient Compton luminosity and the highest gamma-ray energy. In this limit,  $\gamma_{\text{max}}$  is about  $2 \times 10^9$  and the inverse Compton SED shows a steep cut off at  $\sim 10^4$  TeV for  $\mathcal{D} = 10$  if electron-positron pair production is neglected. Note that  $t_{\text{acc}}$  in reality depends on  $\gamma$ , while we assume  $t_{\text{acc}}$  does not depend on  $\gamma$  and the above values were calculated assuming  $\gamma_f = 10^7$  in equation (4).

The shape of SED has a significant curvature in the TeV region in our calculations. This curvature is in contrast to the observations of TeV gamma-rays from Mrk 421, which are fitted by a power law (Krennrich et al. 1999). Mrk 501, on the other hand, show a curvature in TeV emission (Catanese et al. 1997), and there are models which explain the curvature by intergalactic absorption (e.g., Konopelko et al. 1999; Krennrich et al. 1999). We, however, do not address

these issues in this paper, since we are mainly interested in the temporal behavior of electrons and photons due to electron acceleration in the source.

### 3.3. Dependence on the Injection Rate

The spectral energy distributions of electrons and photons depend on the value of the injection rate  $Q(\gamma)$  in the AR as well. If the value of  $Q(\gamma)$  is larger with the fixed values of  $\gamma_0$ ,  $t_{e,esc}$ , and  $t_{acc}$ , the accumulation of electrons in the CR increases, resulting in the dominance of the Compton component. An example of SED is shown 8, where the electron injection rate in the acceleration smaller by a factor 10 than in the model shown in Figure 2, i.e., electrons are injected at the rate of  $0.01 \text{ electrons cm}^{-3} \text{ sec}^{-1}$ . The peak of the synchrotron component decreases by a factor 10 and that of the Compton component decreases by a factor 100.

### 3.4. Dependence on Magnetic Field

When the size of a cloud and the number density of electrons are fixed, the value of  $\gamma_{max}$  is larger for smaller values of  $B$ , because the synchrotron cooling rate is proportional to  $B^2$ . However, this is not the case in our model, because not only the cooling rate but also  $t_{acc}$  depends on  $B$ . When  $B$  is smaller,  $t_{acc}$  is larger, which results in the larger size of the AR. Because we fix the particle injection rate per unit volume in the AR, the total number of electrons injected into the CR per unit time is larger by the electron number conservation. As a result, the Compton cooling in the CR becomes stronger and the value of  $\gamma_{max}$  becomes smaller. However, the increase or decrease of  $\gamma_{max}$  actually depends on the combination of synchrotron cooling and Compton cooling. Such dependence on  $B$  in the CR is shown in Figure 9; SEDs at  $t = 10R/c$  are compared for  $B = 0.05$ ,  $0.1$ , and  $0.5 \text{ G}$  with the same values of other parameters as in Figure 2. In the CR, the values of  $\gamma_{max}$  are  $8 \times 10^6$ ,  $4 \times 10^6$ , and  $8 \times 10^5$  for  $B = 0.05$ ,  $0.1$ , and  $0.5 \text{ G}$ , respectively.

### 3.5. Termination of Acceleration

It is conceivable that acceleration is terminated by the end of electron injection in the AR due to the change of shock structure, etc., so that plasmas cease to emit hard photons. To exemplify such a situation, we continue the injection and acceleration up to  $t = 4R/c$  with the parameters used in Figure 1 and terminate the injection and the acceleration abruptly at  $t = 4R/c$ , while the simulation is continued until  $t = 7R/c$ . A break of the power-law spectrum of electrons in the AR appears after acceleration is terminated, and the break moves to lower energy with time. The response of the emission spectrum to the termination of acceleration is almost simultaneous in different energy bands as shown by light curves in Figure 10. It is observed that the decay at  $0.5 - 2 \text{ keV}$  band lags that at  $2 - 40 \text{ keV}$ , which is characteristic to the models that assume the



injection of power-law electrons and a sudden termination of injection. The decay in the keV range and 1 – 10 TeV bands is exponential, because the supply of the electrons producing those photons is turned off. On the other hand, electrons producing GeV photons are still supplied for a while by the cooling of the highest energy electrons which produced 1 – 10 TeV photons.

### 3.6. Flare

Up to now, we have assumed that at the initial stage the cloud is empty and there are no high energy electrons or photons. This is certainly an over simplification. Many flare events have been observed in X- and gamma-ray ranges by ASCA, Whipple, etc. They are overlaid on a steady emission component. As an example of applications of our code, a flare is simulated, i.e., we simply change the value of  $t_{\text{acc}}$  for a period of time. More specifically, at  $t = 0$  the distributions of electrons and photons are in the steady state which is obtained for the parameters used in §3.1; see the dashed curve in Figure 2 for the steady photon energy distribution. The steady state is still continued for  $R/c$ . We then replace  $t_{\text{acc}}$  by  $t_{\text{acc}}/1.2$  for  $t = R/c - 2R/c$  (about 14 hours in the observer’s frame); after  $t = 2R/c$ , the original value of  $t_{\text{acc}}$  is used. The electron escape time in the AR is also changed keeping  $t_{e,\text{esc}} = t_{\text{acc}}$ . In Figure 11, light curves are shown for such a flare. The response of the light curves to the change of  $t_{\text{acc}}$  (on/off of a flare) is slightly delayed, because of photon production and Compton scattering time. It is also noticed that the change of the light curve at 1 – 10 GeV band delays behind X-rays and TeV gamma-rays. This is a result of an interplay of the time evolution of electron and synchrotron photon spectra. It is shown that the light curves of 2 – 10 and 10 – 40 keV proceed that of 0.5 – 2 keV. This behavior is different from that shown in Figure 3, where the initial condition was an empty blob.

The trajectories in the energy flux and photon index are shown in Figure 12 for  $t = 0 - 10R/c$ . This behavior is qualitatively similar to observed one for Mrk 421 by ASCA (Takahashi et al. 1996). Though the amplitudes of the change in the photon index of 2 – 10 keV and its energy flux are different from those of the observation, these values are dependent on parameters such as  $t_{\text{acc}}$  and the duration of the flare, etc.

## 4. SUMMARY

Simulations of the time evolution of electron and photon energy distributions were presented as a model of time variations observed by X- and gamma-rays from blazars. By assuming that acceleration and cooling regions in a blob are spatially separated, we calculated the energy spectra of electrons in each regions. Electrons in the acceleration region are accelerated with a characteristic timescale  $t_{\text{acc}}$  and escape on a timescale  $t_{e,\text{esc}}$ ; here we assumed  $t_{\text{acc}} = t_{e,\text{esc}}$ , so that the electron spectrum in a steady state obeys a power law,  $N(\gamma) \propto \gamma^{-2}$ , as realized in the standard model of shock acceleration (e.g., Druly 1983; Blandford & Eichler 1987). Electrons escaping from the

acceleration region are injected into the cooling region where they lose energy by radiation and finally escape from the blob on a timescale assumed to be  $2R/c$ . With these assumptions, we performed the simulations of the time evolutions of electrons and photons for various values of parameters. Although we did not include a specific acceleration mechanism, we took into account the salient features of diffusive shock acceleration, so that we could study the properties of time variation accompanying shock acceleration.

We first presented the results of the time evolution of the spectral energy distribution of radiation associated with the evolution of the electron number spectrum. In the early stage of the evolution, i.e.,  $t = 0 - R/c$ , the synchrotron component dominates the spectrum. The energy flux of soft X-rays starts to rise earlier than that of hard X-rays. Later ( $t > R/c$ ), the Compton luminosity gradually increases. At the same time, the peak energy of the synchrotron component decreases because of radiative cooling. It was found that in a steady state, escaping electrons carry more energy than radiation: This result, of course, depends on the values of the parameters used. We also showed the dependence of time evolution on the acceleration timescale, the electron injection rate, and the strength of magnetic fields. The value of  $\gamma_{\max}$  and the ratio of the synchrotron luminosity to the Compton luminosity depend on such parameters.

We next simulated a flare by simply changing the value of  $t_{\text{acc}}$  for a certain time span. With a shorter acceleration timescale, more energetic electrons are produced and consequently more hard photons are produced. The relation between the energy flux and the photon index during a flare was obtained, which is similar to the one observed from Mrk 421 (Takahashi et al. 1996).

Our formulation provides a method to treat high energy flares including particle acceleration processes, which is beyond usual analyses where nonthermal electron spectra are arbitrarily assumed and only cooling processes are included. Although we have not applied our model to any specific case of flares, it is straightforward to do this using our code. The examples presented here seem to cover a wide range of observed flares. These applications are deferred to future work. On the theoretical side, as proposed by Kirk et al. (1998), electrons accelerated at a shock are transferred outside of the shock and cool radiatively. To include such spatial transfer of electrons, we, in future, need to solve for the structure around acceleration regions.

Recently Chiaberge & Ghisellini (1999) showed observational consequences associated with time variations with timescales shorter than  $R/c$ . When such short timescale variations occur, observed emission is a superposition from various parts of a cloud. Then the time profile of each time variation is not necessarily observed clearly. The model presented in this paper contains the acceleration timescale shorter than  $R/c$ . Thus our model may not directly reflect observed spectra. However, to understand the relation between electron acceleration and time variation of emission, such a study should be useful.

M.K. and F.T. have been partially supported by Scientific Research Grants (M.K.: Nos. 09223219 and 10117215; F.T.: Nos. 09640323, 10117210, and 11640236) from the Ministry of

Education, Science, Sports and Culture of Japan.

## REFERENCES

- Blandford, R. D., & Coppi, P. S. 1990, MNRAS, 245, 453
- Blandford, R., & Eichler, D. 1987, Phys. Rep., 154, 1
- Blandford, R. D., & Königl, A. 1979, ApJ, 232,34
- Blandford, R. D., & Rees, M. J. 1978, in Pittsburgh Conf. on BL Lac Objects, ed. A. M. Wolfe (Pittsburgh: Univ. Pittsburgh Press), 328
- Catanese, M. et al. 1997, ApJ, 487, 143
- Chiaberge, M., & Ghisellini, G. 1999, MNRAS, 306, 551
- Crusius, A., & Schlickeiser, R. 1986, A&A, 164, L16
- Drury, L. O. C. 1983, Rep. Prog. Phys., 46, 973
- Gaidos, J. A. et al. 1996, Nature, 383, 319
- Inoue, S., & Takahara, F. 1996, ApJ, 463, 555
- Jones, F. C. 1968, Physical Review, 167, 1159
- Kataoka, J. et al. 1999, ApJ, 514, 138
- Kirk, J. G., Rieger, F. M., & Mastichiadis, A. 1998, A&A, 333, 452
- Konopelko, A. K., Kirk, J. G., Stecker, F. W., & Mastichiadis, A. 1999, ApJ, 518, L13
- Krennrich, F. et al. 1999, ApJ, 511, 149
- Maraschi, L., Ghisellini, G., & Celotti, A. 1992, ApJ, 397, L5
- Mastichiadis, A., & Kirk, J. G. 1995, A&A, 295, 613
- Mastichiadis, A., & Kirk, J. G. 1997, A&A, 320, 19
- Mukherjee, R. et al. 1997, ApJ, 490, 116
- Robinson, P. A., & Melrose, D. B. 1984, Australian J. Physics, 37, 675
- Sikora, M., Begelman, M. C., & Rees, M. J. 1994, ApJ, 421, 153
- Takahashi, T., Tashiro, M., Madejski, G., Kubo, H., Kamae, T., Kataoka, J., Kii, T., Makino, F., Makishima, K., & Yamasaki, N. 1996, ApJ, 470, L89

Ulrich, M.-H., Maraschi, L., & Urry, C. M. 1997, *ARA&A*, 35, 445

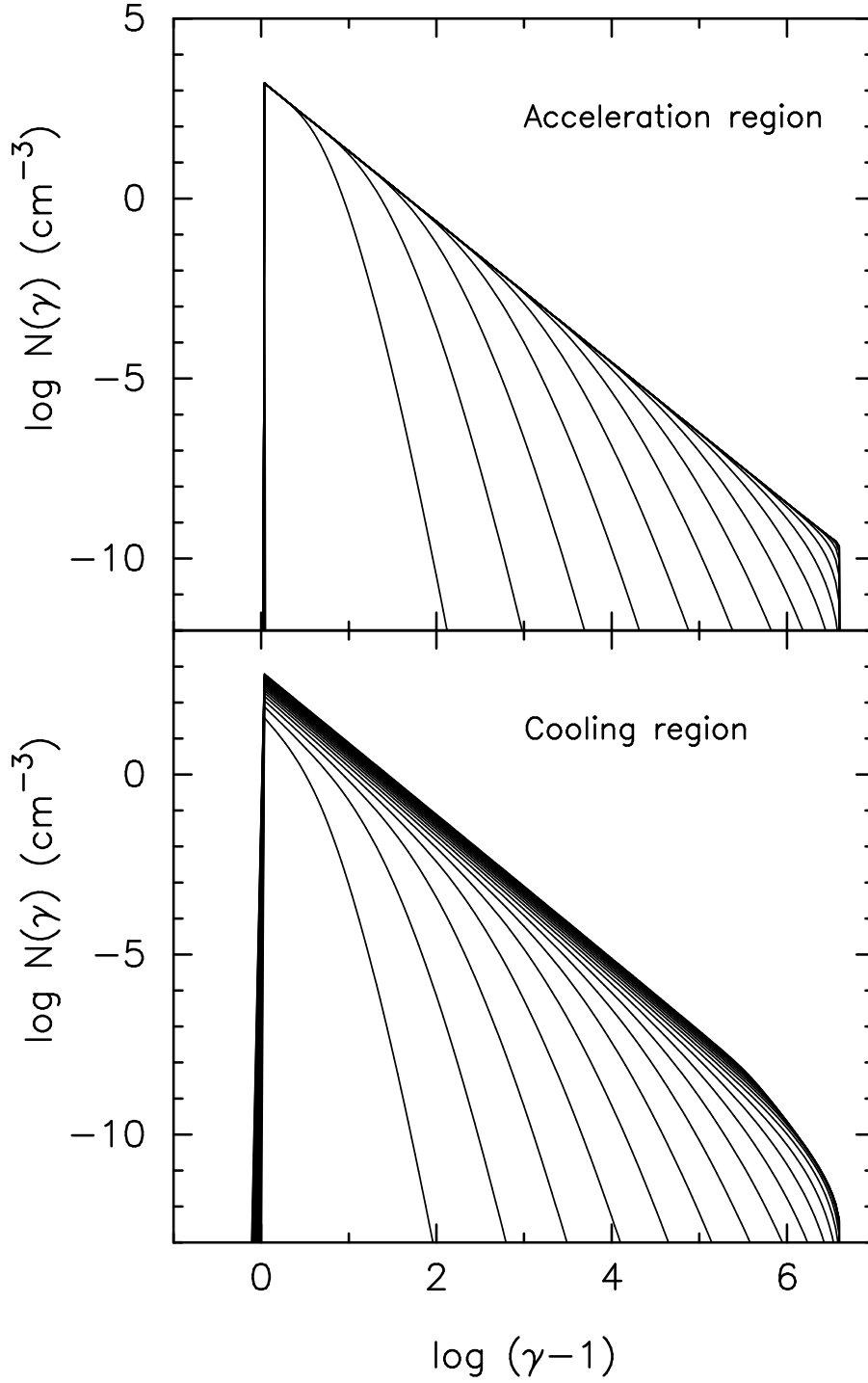


Fig. 1.— Time evolution of electron number spectra in the acceleration (upper panel) and cooling (lower panel) regions for  $t = 0 - R/c$  with the equally spaced time span of  $0.05R/c$ . The spectra evolve from lower to upper curves in each panel.

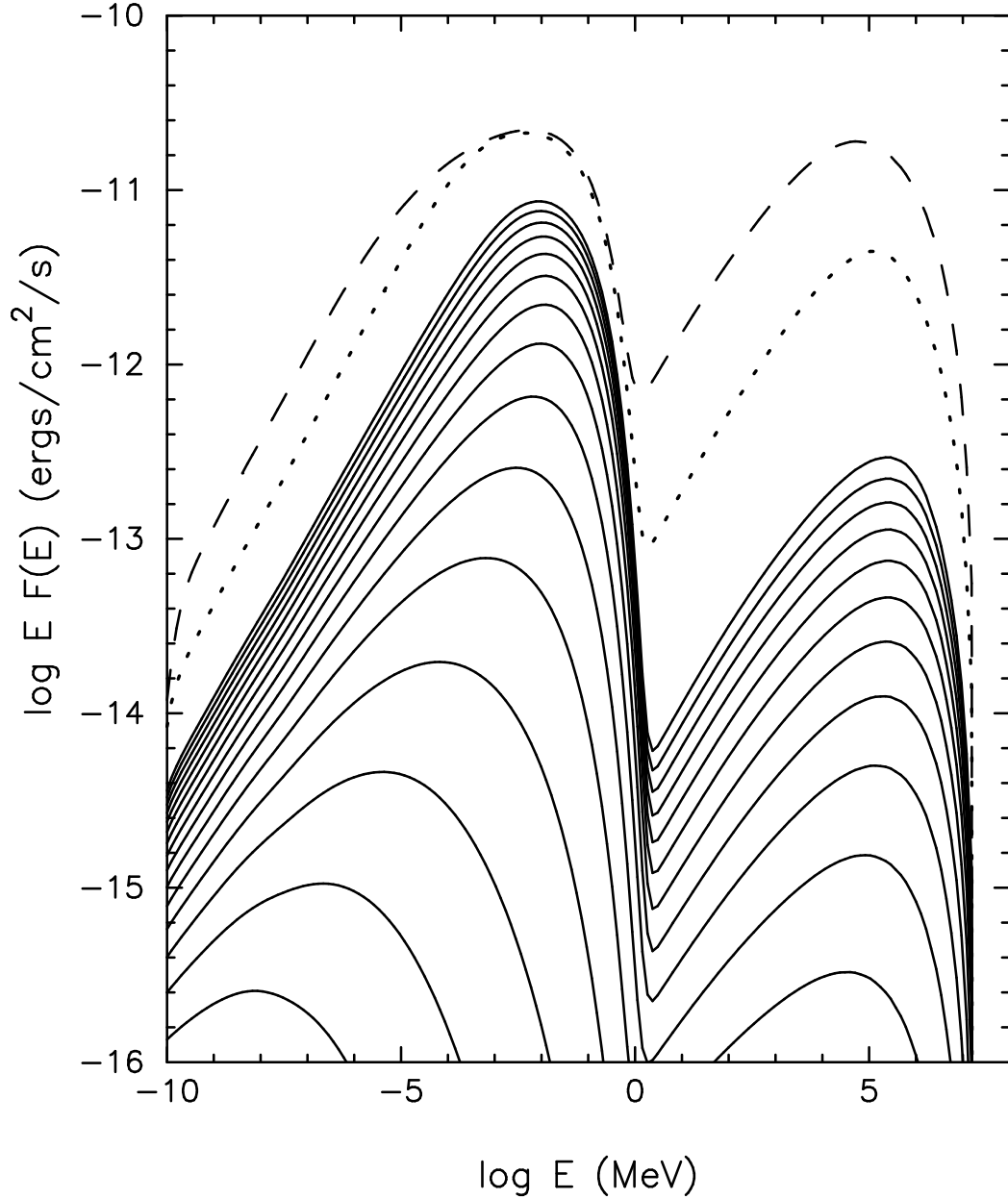


Fig. 2.— Time evolution of the spectral energy distribution (SED) of photons emitted by electrons in the cooling region shown in Figure 1; SED is shown in the observer’s frame. The solid curves are for  $t = 0 - R/c$  (lower to upper curves) with the equally spaced time span of  $0.05R/c$ . SEDs when the simulation is continued after  $R/c$  with continuous injection and acceleration are also shown; the dotted curve shows SED at  $t = 2R/c$  and the dashed curve is SED at  $t = 10R/c$ , at which the radiation is already in a steady state.

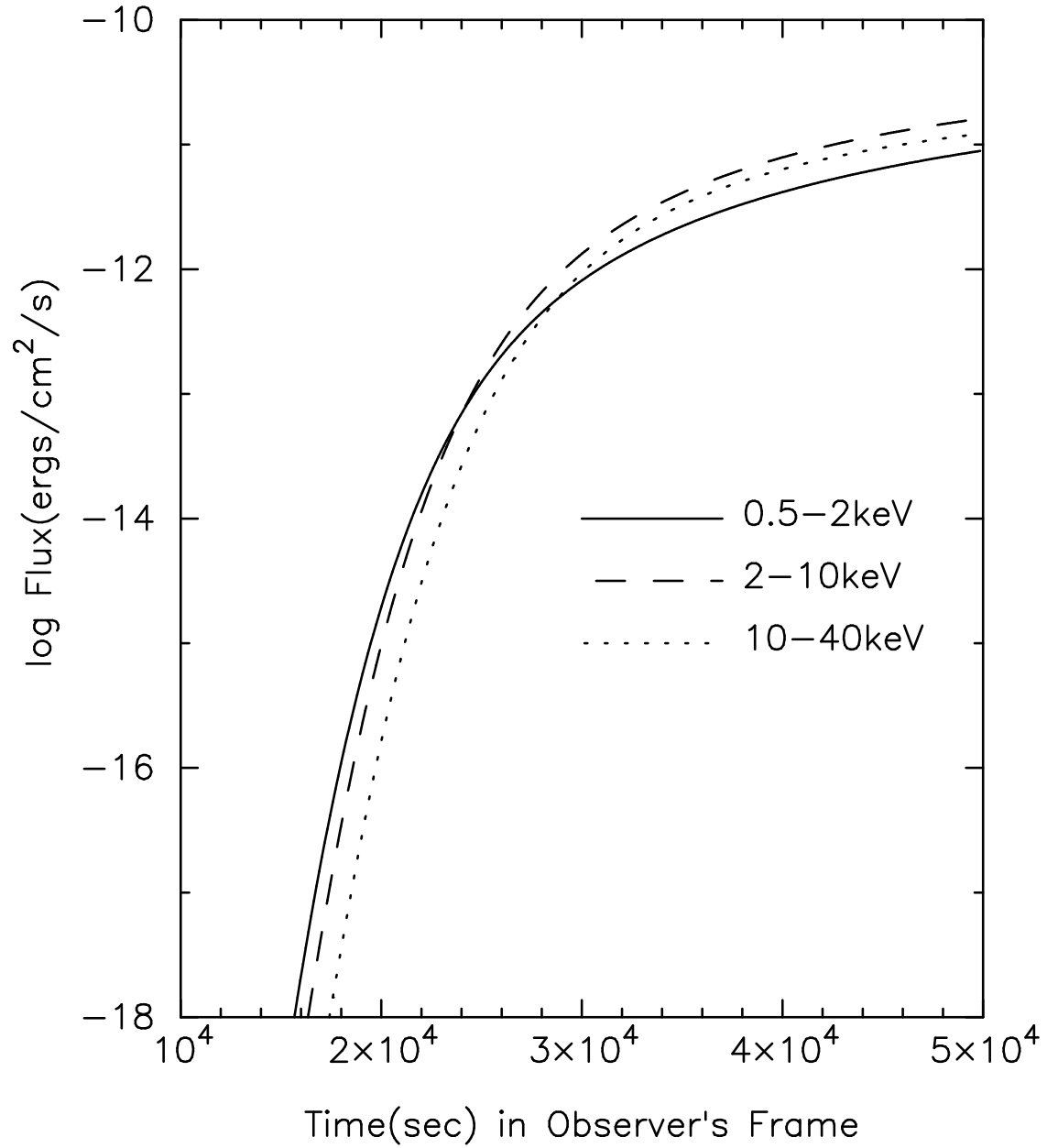


Fig. 3.— Light curves for 0.5 – 2, 2 – 10, and 10 – 40 keV bands. The energy flux of soft X-rays is larger than that of hard X-rays for  $t \lesssim 15t_{\text{acc}}$ .

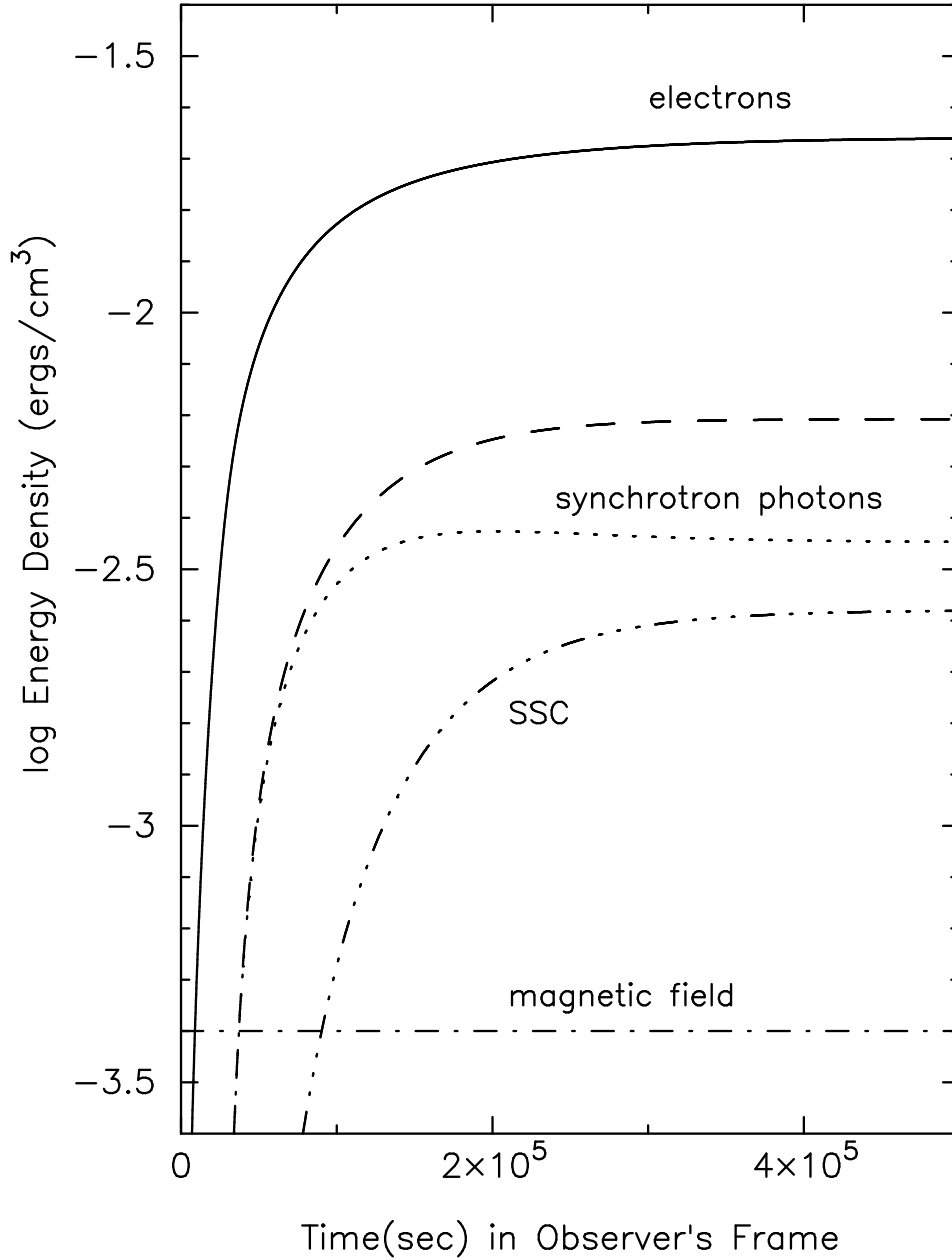


Fig. 4.— Time evolution of the energy densities of electrons and photons in the cooling region. Here the strength of magnetic field is fixed,  $B = 0.1$  G. Curves are plotted for  $t = 0 - 10R/c$ , where  $R/(c\mathcal{D}) = 5 \times 10^4$  sec and  $t_{\text{acc}}/\mathcal{D} \approx 2 \times 10^3$  sec in the observer's frame. Solid curve: electrons, long-dashed: photons (synchrotron plus SSC), dotted: synchrotron photons, dash-dot-dot-dotted: SSC photons, and dash-dotted: magnetic field.



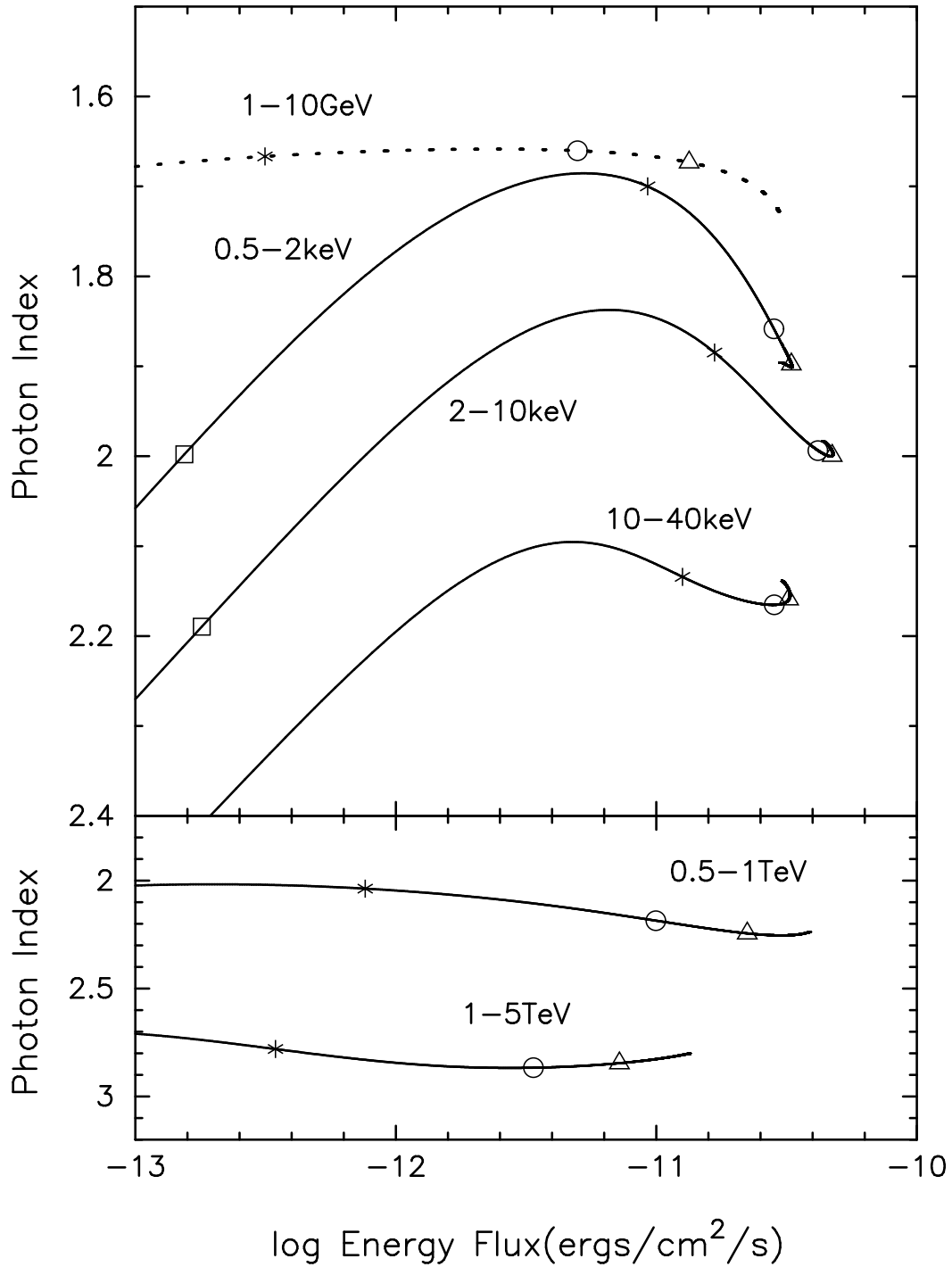


Fig. 5.— Trajectory in the energy-flux and photon-index plane for various energy bands. The evolution is calculated for  $t = 0 - 10R/c$ . Symbols on the curves indicate the time from  $t = 0$ ;  $t = 0.5R/c$  (squares),  $R/c$  (asterisks),  $2R/c$  (circles), and  $3R/c$  (triangles).

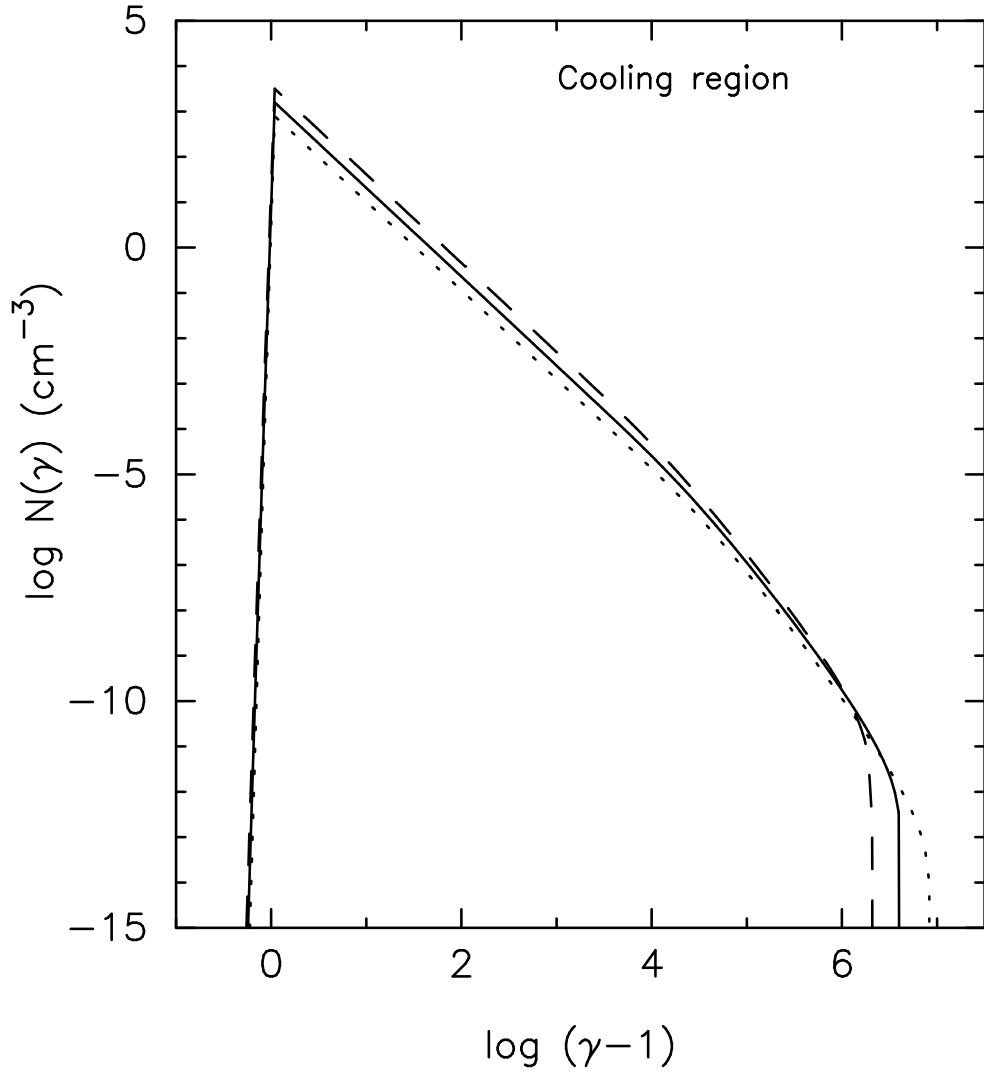


Fig. 6.— Electron distribution in the cooling region at  $t = 10R/c$  for various values of the acceleration timescale. The solid curve is for  $\xi = 5 \times 10^2$ , the dashed curve for  $\xi = 10^3$ , and the dotted curve for  $\xi = 2.5 \times 10^2$ .

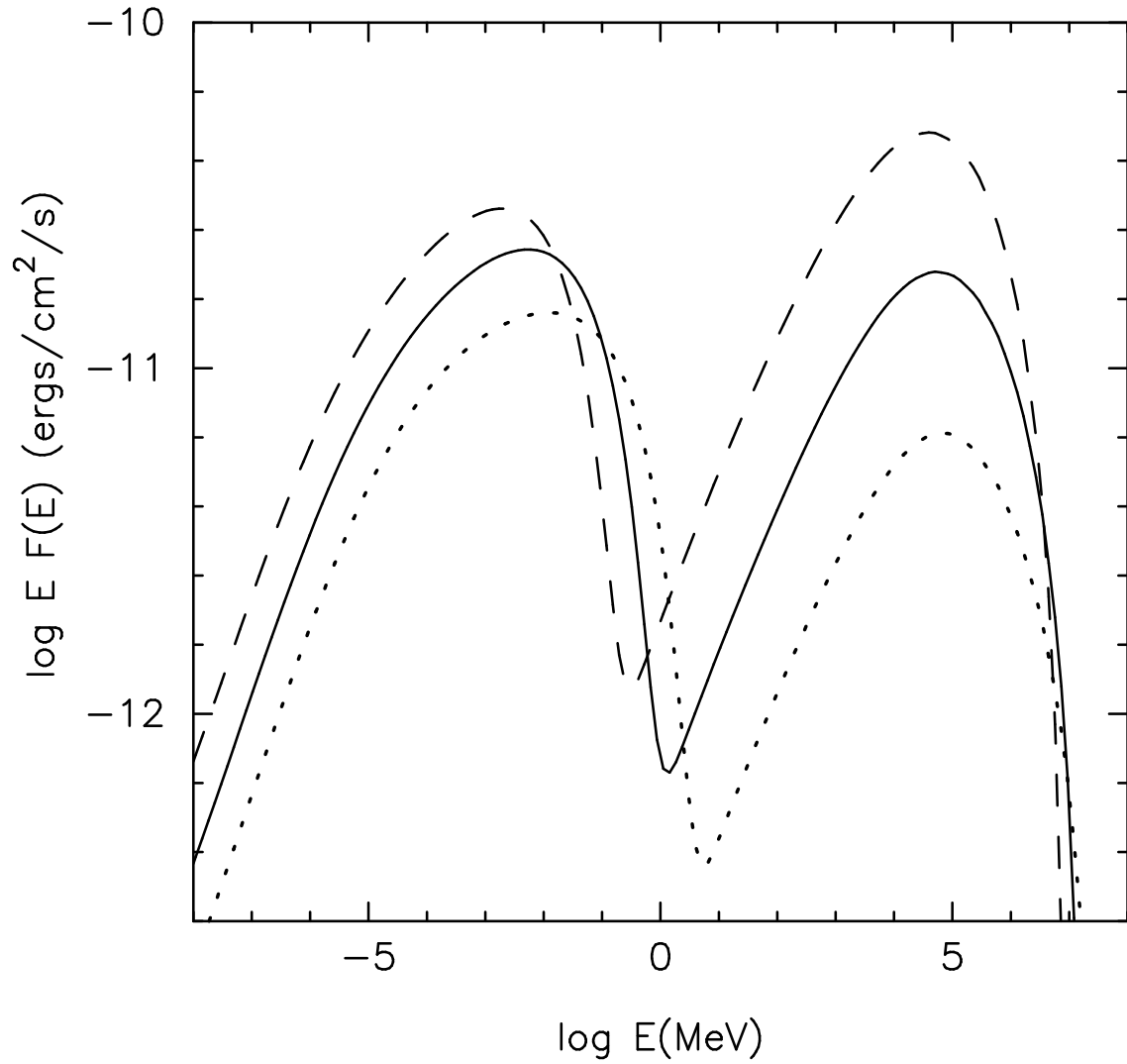


Fig. 7.— SDEs at  $t = 10R/c$ , corresponding to Figure 6, for various values of the acceleration timescale. The solid curve is for  $\xi = 5 \times 10^2$ , the dashed curve for  $\xi = 10^3$ , and the dotted curve for  $\xi = 2.5 \times 10^2$ .

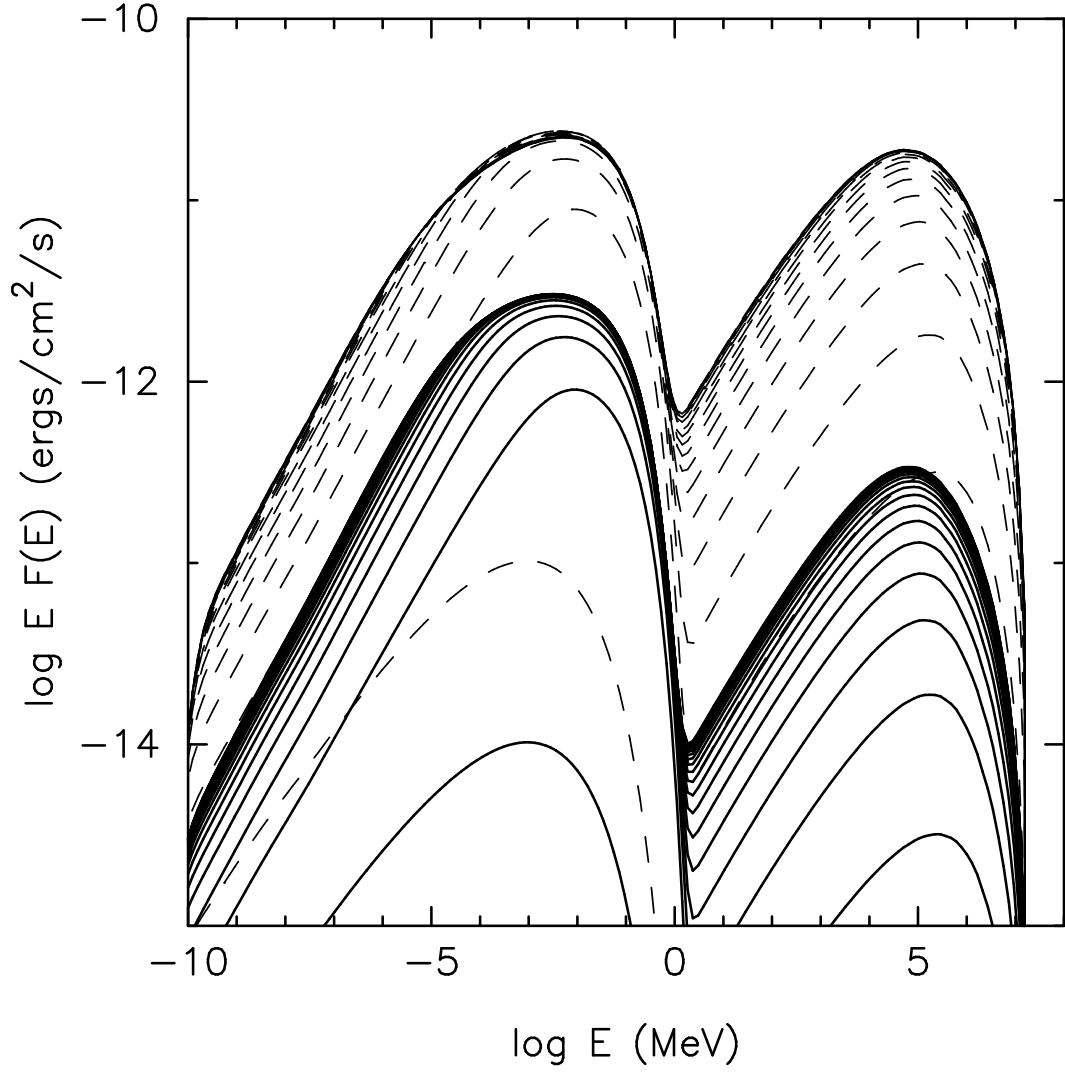


Fig. 8.— Evolution of SEDs for different values of  $Q(\gamma)$ . The solid curves are the evolution of SED with  $Q(\gamma)$  smaller by a factor 10 than that of Figure 2 shown here by the dashed curves. The curves are plotted for  $t = 0 - 10R/c$  with the time interval  $0.5R/c$  and evolve from lower to upper.

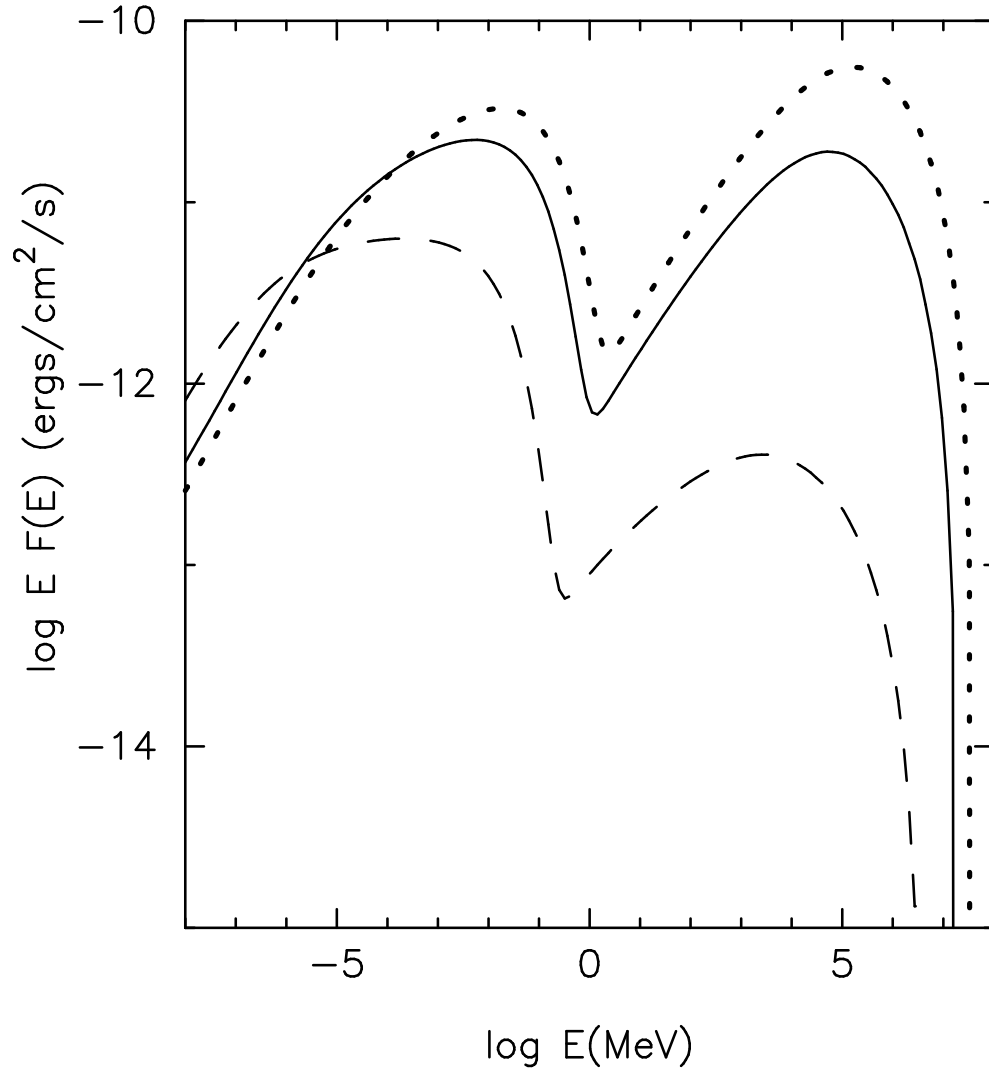


Fig. 9.— SED at  $t = 10R/c$  for different values of  $B$ . The solid curve is SED for  $B = 0.1$  G (the same curve as shown in Figure 2), the dotted curve is SED for  $B = 0.05$  G, and the dashed curve is for  $B = 0.5$  G.

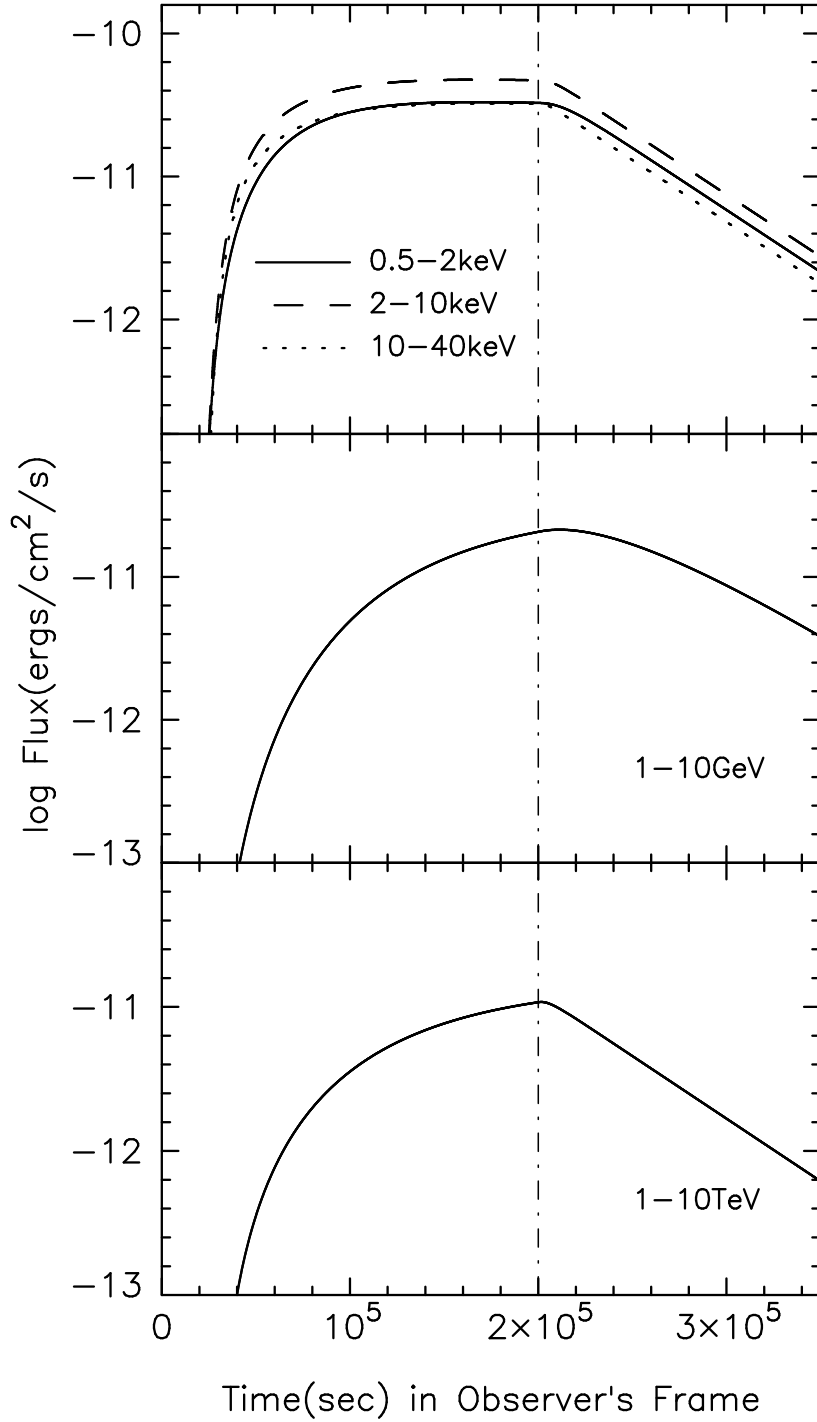


Fig. 10.— The response of light curves to the termination of acceleration. Acceleration and injection are terminated at  $4R/c$  or  $2 \times 10^5$  sec in the observer's frame, shown by the vertical dash-dotted line. Parameters are the same as in Figure 1.

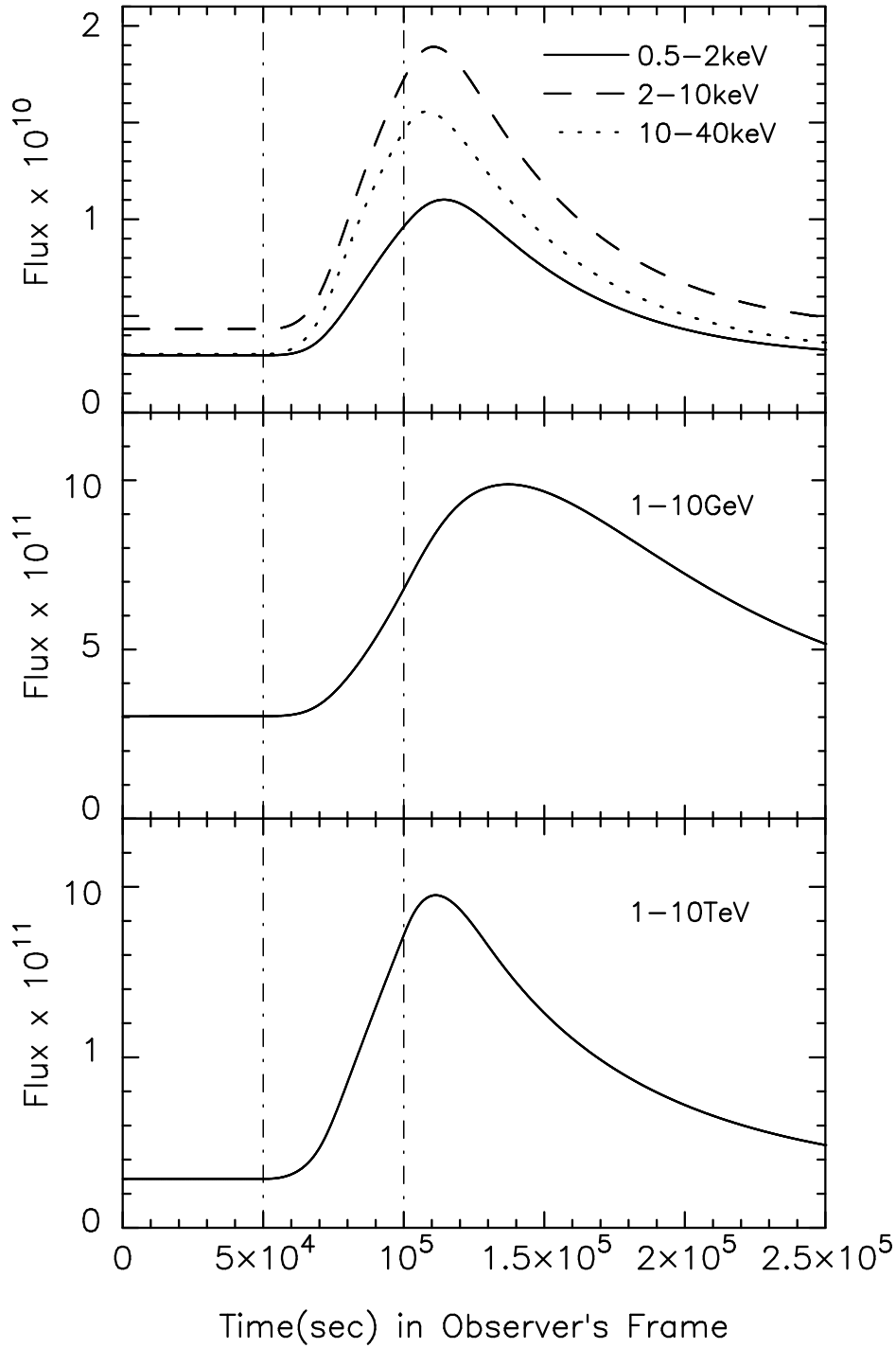


Fig. 11.— Light curves for  $t = 0 - 5R/c$  including a flare which occurs during  $t = R/c$  and  $2R/c$ , indicated by the vertical dash-dotted lines. The fluxes are in units of  $\text{ergs cm}^{-2} \text{sec}^{-1}$ .

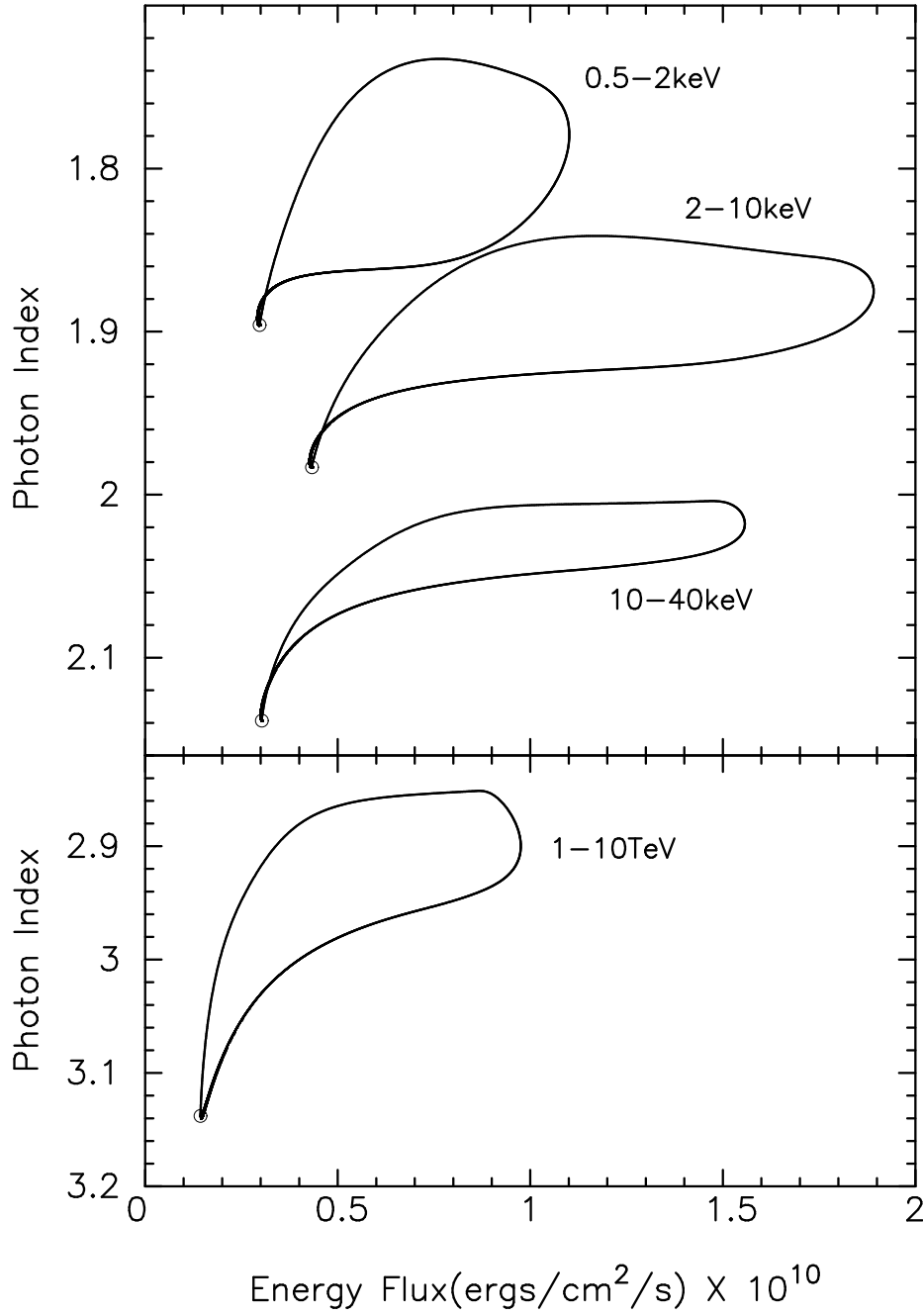


Fig. 12.— Time evolution of the energy flux and the photon index associated with the flare shown in Figure 11; the trajectories start from a steady state (shown by open circles) and rotate clockwise. The evolution is calculated until  $t = 10R/c$ .